Research Square

Preprints are preliminary reports that have not undergone peer review.
They should not be considered conclusive, used to inform clinical practice,
or referenced by the media as validated information.

Trehalose Transport as a Male-Specific Axis of Mosquito Energy Metabolism and Reproductive Fitness

Nirmala Sankhala
National Institute of Malaria Research
Tanvi Singh
National Institute of Malaria Research
Pooja Yadav
National Institute of Malaria Research
Vaishali Saini
National Institute of Malaria Research
Pooja Rohilla
National Institute of Malaria Research
Vartika Srivastava
National Institute of Malaria Research
Gunjan Sharma
National Institute of Malaria Research
Suchi Tyagi
National Institute of Malaria Research
Sanjay Tevatiya
National Institute of Malaria Research
Punita Sharma
National Institute of Malaria Research
Rajnikant Dixit
rkdixit@icmr.gov.in

National Institute of Malaria Research

Article

Keywords: Anopheles stephensi, Trehalose metabolism, Male mosquito fitness, Carbohydrate homeostasis, RNAi, Vector Control Strategies, Reproductive energetics

Posted Date: March 30th, 2026

DOI: https://doi.org/10.21203/rs.3.rs-9119904/v1

License: This work is licensed under a Creative Commons Attribution 4.0 International License.
Read Full License

Additional Declarations: No competing interests reported.

Abstract

Anopheles stephensi is a major urban malaria vector whose expanding range intensifies the need for complementary control tools. While females have been the primary focus of studies on energy metabolism due to their role in blood feeding and parasite transmission, male biology is equally relevant to strategies that exploit reproductive fitness, such as sterile insect technology (SIT) and incompatible insect technology (IIT). Yet male energetics shaped by exclusive dependence on sugar feeding remain inadequately defined, particularly in the context of reproductive performance, which is central to the mosquito population dynamics.

Here, we investigated trehalose metabolism in male *Anopheles stephensi* using survival assays, stage-resolved gene expression profiling, and RNAi-mediated knockdown. Trehalose feeding reduced male longevity by more than half relative to sucrose, whereas females showed smaller shifts from their respective baseline. Expression of the trehalose transporter (*AsTRET*) varied across swarm stages in fat body and midgut, and trehalase displayed stage-linked modulation. While silencing altered circulating trehalose levels and reduced mating-associated egg output. These findings identify trehalose transport and utilization as a key component of male reproductive physiology and highlight carbohydrate homeostasis as a potential target for male-focused vector control strategies.

Introduction

In India, *Anopheles stephensi* is a dominant malaria vector whose success in sustaining malaria transmission cycles depends on its ability to survive and reproduce under diverse ecological conditions [1]. As with all organisms, the persistence of this species ultimately follows Darwin's principle of "survival of the fittest," where reproductive fitness is the key measure of evolutionary success both in terms of quality and quantity. In mosquitoes, reproductive fitness is inseparably linked to nutrition, and the sexes differ sharply in their nutritional strategies [2]. Females are anautogenous, requiring vertebrate blood meals to produce eggs, while males, lacking this option, rely exclusively on plant-derived sugars such as floral nectar to fuel their life processes.[3]

Because males depend solely on sugar metabolism, their reproductive output is critically shaped by how efficiently they regulate sugar homeostasis [4,5]. Central to this regulation is trehalose, the principal circulating sugar in insects, which serves not only as an energy reserve but also as the immediate substrate that fuels swarming and mating activity [6]. The maintenance of trehalose balance is controlled by the trehalose transporter (TRET1), which enables bidirectional mobilization between the fat body, haemolymph, and peripheral tissues [7]. Trehalose synthesized in the fat body is exported into the haemolymph and delivered to high-demand organs such as flight muscle, brain, and reproductive tissues; conversely, TRET1 also mediates reuptake to stabilize circulating levels. Once in target tissues, trehalose is hydrolysed into glucose by trehalase, an enzyme present both in the haemolymph and at the cellular level, supplying an immediate fuel for glycolysis and ATP production [8]. Thus, the coordinated activities of TRET1 and trehalase integrate storage, circulation, and utilization of trehalose, positioning this

transport–hydrolysis axis as a central determinant of male mosquito energetics and reproductive fitness [9,10]

The link between sugar metabolism and swarm energetics in male mosquitoes has been recognized for decades. Classic field studies in *Anopheles freeborni* showed that swarm flight consumes more than half of a male's caloric reserves and is fuelled primarily by trehalose, glucose, and glycogen rather than lipids[6], establishing stored carbohydrates as critical for reproductive success. However, these studies linked swarming to carbohydrate consumption without connecting swarm behaviour to the physiologically active regulatory steps that determine trehalose availability, particularly transport and hydrolysis, during mating. More recent 3D video tracking of laboratory swarms in *Anopheles gambiae* revealed structured swarm organization and pronounced male–male competition [11], indicating that swarm participation involves dynamic competitive interactions likely to impose fluctuating metabolic demands.

Sugar metabolism supports more than flight; it directly shapes male reproductive output. In *Aedes aegypti*, males and females exhibit synchronized peaks in sugar feeding, and male mating activity rises and falls with these feeding rhythms [12]. Sugar-deprived males die within days and fail to mate, whereas sugar-fed males survive longer and continue inseminating females [3,13]. Together, these findings suggest that carbohydrate availability constrains both endurance and mating performance. Yet the mechanisms governing trehalose transport and hydrolysis in *An. stephensi* males, and their connection to reproductive success, remain unaddressed.

Resolving this gap is important not only for understanding male energetics but also for applied vector control. Strategies that depend on male mating competitiveness, including sterile insect approaches and male-drive female-sterile systems[14], assume that engineered males can effectively compete within swarms. Defining how trehalose metabolism underpins male performance, therefore links basic reproductive physiology to the efficacy of emerging genetic control programs.

Building on the premise that male mosquitoes operate close to an energetic threshold, where carbohydrate quality may directly constrain survival and mating capacity, we tested whether regulation of trehalose transport and hydrolysis underlies male reproductive performance in *An. stephensi*. Consistent with this framework, trehalose feeding reduced male survival by more than half relative to sucrose, whereas females showed comparatively modest shifts from their sex-specific baseline. Across mating stages, *TRET1* expression dynamically changed in fat body and midgut, and trehalase displayed stage-specific induction during swarm activity, indicating coordinated regulation of trehalose mobilization and utilization. Functional disruption of TRET1 perturbed haemolymph trehalose homeostasis, and was accompanied by reduced mating output. Together, these findings position the trehalose transport–hydrolysis axis as a critical regulator of male energetic balance and reproductive performance, linking carbohydrate homeostasis to swarm competitiveness and providing a physiological relevance to male-dependent vector control strategies.

Results

Molecular Characterization of the A. stephensi Trehalose Transporter (AsTRET1)

To confirm the molecular identity of the transporter examined in functional assays, the *A. stephensi* TRET1 gene (ASTE010234) was annotated and characterized in silico. The predicted protein (842 aa) contained a conserved Major Facilitator Superfamily (MFS) domain with 12 transmembrane helices, along with canonical GLUT6/8-like signatures and multiple putative substrate-binding motifs (Fig. 1-a). Structural prediction using AlphaFold2 showed the expected MFS fold, with inward–outward alternating topology typical of sugar porters (Fig. 1-b). Phylogenetic analysis placed *An. stephensi* TRET1 within a well-supported clade of mosquito trehalose transporters, grouping closely with *An. minimus*, *An. funestus*, and *An. coluzzii* (Fig. 1-c). Node support was assessed using a maximum-likelihood framework with 100 bootstrap replicates. These features confirm that the locus targeted in expression and RNAi assays corresponds to a conserved insect trehalose transporter.

Differential Survival Under Sugar Diets Reveals a Male-Biased Metabolic Vulnerability, Modulated by Mating Status

Adult males and females were maintained on defined sugar diets and monitored daily to assess longevity (Fig. 2a). Sucrose served as the control diet, trehalose as the principal circulating sugar in insects, and xylitol and erythritol as non-nutritive sugar alcohols. Kaplan–Meier survival analysis revealed clear differences between diets (Fig. 2d). Males maintained on sucrose survived for a mean of 20.3 days. In contrast, males fed trehalose showed reduced longevity at all concentrations tested. Mean survival declined to 11 days at 2 and 5 percent trehalose and to 9 days at 10 percent, with corresponding shifts in survival curves (Fig. 2c,d). Females displayed a lower baseline survival on sucrose (13.7 days). Trehalose feeding at 2 and 5 percent did not markedly alter female survival relative to sucrose, whereas 10 percent trehalose resulted in a moderate reduction to 11 days (Fig. 2c,d). The sugar alcohols produced distinct but non–sex-specific outcomes (Fig. 2c). Erythritol caused rapid mortality in both males and females, with all individuals dying within approximately three days across concentrations. Xylitol induced a concentration-dependent decrease in lifespan in both sexes, with mean survival ranging from 6–11 days in males and 7–14 days in females. The magnitude of the survival shift from the respective sucrose baselines differed between sexes for trehalose, whereas erythritol and xylitol produced comparable reductions relative to control in males and females.

To assess whether reproductive status independently influenced longevity, virgin and mated mosquitoes of both sexes were maintained on 10 percent sucrose under identical conditions (Fig. 2b). Mating significantly reduced median longevity in both sexes (Fig. 2c). Virgin males exhibited a median survival of 15 days, whereas males housed with sugar-fed females showed a reduced median of 12.5 days ($p < 0.001$). A more pronounced effect was observed in females: virgin females survived for a median of 16 days, compared with 10 days for females housed with sugar-fed males ($p < 0.0001$), representing a 37.5 percent reduction in median lifespan. These results indicate that the energetic demands associated with

mating impose a measurable survival cost, with females sustaining a disproportionately greater reduction in longevity following copulation. Together, these data demonstrate that both dietary composition and mating status independently modulate adult mosquito lifespan, and suggest that the interplay between metabolic constraint and reproductive investment may contribute to the observed sex-specific differences in survival.

Transcriptional Shifts in Trehalase and TRET1 Across the Swarm–Mating Continuum

To determine whether trehalose regulation varies across the reproductive sequence, TreT and TreH expression were quantified in males sampled at five defined stages: Control (resting), Preswarm, Active swarm, Coupled (mating pairs collected during genital engagement; see Supplementary Video), and Post-swarm. TreT exhibited stage- and tissue-specific variation (Fig. 3a–c).

In the midgut, TreT expression was highest at the preswarm stage and declined through active swarm, coupling, and post-swarm. Expression at post-swarm was significantly lower than at preswarm ($p = 0.045$; Fig. 3b-i). In the fat body, TreT expression increased at preswarm, decreased during active swarm, and reached its highest levels in coupled males before returning toward control levels post-swarm. Coupled males showed significantly higher fat body TreT expression than preswarm males ($p = 0.038$; Fig. 3b-ii).

Midgut expression profiles of TreH and TreT revealed additional stage-linked differences (Fig. 3d). TreH expression was highest during the active swarm stage, whereas TreT levels in the midgut showed comparatively smaller variation across stages.

Stage-Linked Fluctuations in Trehalose Pools During Male Reproductive Activity

To determine whether circulating carbohydrate pools vary across the male reproductive sequence, haemolymph was collected from males sampled at defined swarming and mating stages and analysed using an enzymatic trehalose assay (Fig. 4a). Trehalose concentrations were quantified following trehalase digestion and glucose detection, using replicate-specific standard curves within the linear range of the assay (Fig. 4b). Analysis of haemolymph trehalose-to-glucose ratios across stages revealed stage-dependent differences (Fig. 4c). Control, Pre-swarm, Active swarm, and Post-swarm males showed comparable ratios, whereas Coupled males exhibited a significantly higher trehalose-to-glucose ratio relative to Control ($p < 0.05$). No other stage comparisons reached statistical significance.

To examine individual carbohydrate pools, pairwise comparisons were performed using linear mixed-effects models (Fig. 4d). Total glucose concentrations did not differ significantly between Control and Post-swarm males (Fig. 4d-i; $p = 0.5388$). In contrast, haemolymph trehalose levels were lower in Post-

swarm males compared to Controls (Fig. 4d-ii; p = 0.01928). Endogenous glucose concentrations varied across Control, Coupled, and Post-swarm stages, with significant pairwise differences detected where indicated (p < 0.05; Fig. 4d-iii), while other comparisons were not significant.

Disrupting Trehalose Transport Alters Circulatory Balance and Tissue Uptake

To assess the effects of reduced trehalose transport, TreT expression was decreased in adult males by dsRNA-mediated gene silencing and quantified in fat body tissue 48 h post-injection (Fig. 5a). TreT transcript levels were significantly lower in silenced males compared to controls (Welch's t-test: t = 2.62, df = 7.36, p = 0.033; Fig. 5b-i). Haemolymph was collected from control, TreT-silenced, and TreH-silenced males and analysed using the trehalase-based enzymatic assay (Fig. 5b-ii). TreT-silenced males exhibited higher haemolymph trehalose concentrations than controls ($p = 2.1 \times 10^{-4}$). TreH-silenced males showed higher trehalose levels than both control and TreT-silenced groups ($p = 6.4 \times 10^{-5}$). These differences were consistent across biological replicates.

To evaluate reproductive output, egg production was quantified in females mated with control or TreT-silenced males (Fig. 5c). Across paired replicates, females mated with TreT-silenced males produced fewer eggs than those mated with control males (paired Student's t-test: t = − 3.19, df = 31, p = 0.0033; Wilcoxon signed-rank test: p = 0.0024; Fig. 5d). The mean reduction in egg output was approximately 20–22% (Cohen's d = 0.69). No significant difference was observed in the number of unlaid eggs between groups.

Combined silencing of TreT and TreH further reduces male reproductive output

TreT and TreH were simultaneously silenced in adult males using dsRNA-mediated knockdown, and female egg production following mating with control or double-silenced males was quantified across three independent biological replicates (Fig. 6a). In each replicate, females mated with double-silenced males produced fewer eggs than those mated with control males. When pooled, total egg output was reduced by 33.1% in the double-silenced group relative to controls (Fig. 6b). This difference was statistically significant (**p < 0.001) with a large effect size (Cohen's d = 0.8). Knockdown efficiency was assessed for both targets following double silencing (Fig. 6c). Whole-body TreH expression was reduced by 62.7% relative to controls (p = 0.21), and fat body TreT expression was reduced by 36.6% (p = 0.47).

Discussion

Male *Anopheles stephensi* occupy a uniquely constrained metabolic niche. Unlike females, which supplement sugar-derived energy with blood meals, males rely entirely on plant carbohydrates to sustain maintenance, flight, swarming, copulation, and sperm transfer [15], [5 [16]. In insects broadly, trehalose

functions as the principal circulating sugar and a rapidly mobilizable glucose reserve [17]. Its evolutionary antiquity and centrality to insect metabolism have been traced across insect lineages [18]. Yet despite its recognized role as a flight fuel [6][19], the behavioural regulation of trehalose flux in male mosquitoes has remained unclear. We identify a stage-dependent trehalose axis in which hydrolysis predominates during swarm flight, redistribution increases at coupling, and transport capacity is essential for maintaining haemolymph enantiostasis and reproductive performance.

The dietary survival assays reveal that the sexes do not start from the same longevity baseline, and that difference matters for interpreting sugar effects. On sucrose, males lived longer than females (20.3 vs 13.7 days), establishing a higher baseline reserve for males under control conditions. Against these sex-specific baselines, trehalose produced a distinctly male-biased survival cost. Male longevity dropped sharply on trehalose at every concentration tested, falling to 11 days at 2% and 5%, and to 9 days at 10%. Females, in contrast, showed little change at 2% and 5% trehalose relative to their sucrose baseline, with only a moderate reduction at 10%. Thus, the major contrast lies in the magnitude of deviation from the control baseline, indicating that males are more sensitive to how trehalose is processed rather than to sugar exposure per se.

This male-specific sensitivity is not explained by generalized dietary toxicity. Erythritol produced rapid mortality in both sexes, consistent with previous work in mosquitoes showing that erythritol feeding reduces trehalose, glycogen, and lipid stores, leading to starvation-like collapse [20]. Xylitol similarly shortened lifespan in both sexes. Trehalose's role as a regulated haemolymph reserve has been demonstrated across insect systems. In Drosophila, absence of trehalose does not block development but causes extreme starvation sensitivity [21], highlighting its function as a metabolic buffer. In lepidopterans, disruption of trehalose metabolism depletes systemic energy metabolites [22]. These studies, although conducted in other insect taxa, reinforce a general principle: survival depends on regulated access to trehalose reserves rather than simple sugar ingestion. In male mosquitoes, whose reproductive activity depends entirely on carbohydrate-derived energy, perturbation of this regulatory axis appears particularly consequential.

The survival phenotype therefore justified a male-focused mechanistic analysis. Although trehalose-linked reproductive trade-offs have been described in Loxostege (Lepidoptera), where ovarian Tret1 expression increases under high temperature [23] that context involves stress-induced allocation to female reproductive tissues. In male mosquitoes, the principal energetic challenge is behavioural: sustained swarm flight followed by copulation must be fuelled exclusively by circulating carbohydrate reserves [15], [3]. The longevity data from the mating-status assay are consistent with this framework but reveal that the cost is not equally interpretable across sexes.

In females, the substantial reduction in mean longevity following mating (16 to 10 days) cannot be attributed to a single physiological cost, as mated females engage in host seeking, vitellogenesis, and oviposition; each imposing independent metabolic demands that confound isolation of the direct

energetic cost of copulation[2]. In males, by contrast, the reduction upon mating (15 to 12.5 days) can be more parsimoniously linked to the energetic expenditure of copulation itself, given the absence of comparable post-mating physiological commitments[4]. Males neither blood-feed nor provision offspring; their reproductive investment is concentrated in swarming and copulation, and the observed survival cost likely reflects depletion of carbohydrate reserves allocated to these behaviours. The survival phenotype therefore justified a male-focused mechanistic analysis, beginning with transcriptional profiling of trehalose-pathway genes across the swarm–mating sequence.

Across defined swarm stages, trehalose handling is re-timed rather than held constant. Trehalase expression peaks during active swarming, consistent with rapid trehalose-to-glucose conversion supporting flight metabolism [6]. During coupling, fat body TreT expression increases and the haemolymph trehalose-to-glucose ratio rises specifically at this stage, placing redistribution at copulation rather than flight alone. This pattern aligns with the concept of enantiostasis, originally articulated across insects [24] [9], in which functional stability is maintained despite fluctuations in internal variables. Here, circulating trehalose levels are allowed to shift across behavioural states while reproductive performance is preserved (Fig. 7). Such controlled fluctuation is consistent with evidence from lepidopterans that haemolymph trehalose is maintained through continuous dynamics of synthesis, degradation, and redistribution [19]

If trehalose dynamics across the swarm sequence represent regulated redistribution rather than simple accumulation, then interference with TreT should uncouple circulating levels from tissue access. We tested this directly through targeted silencing of TreT in adult males.

Trehalose functions in insects as a circulating glucose sink that buffers energy demand and releases glucose upon hydrolysis [17]. Its concentration in haemolymph is not simply a reflection of dietary intake but is maintained through regulated transport and enzymatic turnover. When TreT expression was reduced in *A. stephensi*, circulating trehalose rose significantly, indicating that trehalose export from storage tissues continued but tissue uptake was impaired. This interpretation aligns with the functional characterization of TreT1 in the sleeping chironomid (*Polypedilum vanderplanki*), where direct trehalose transport into cells was demonstrated [25]. Blocking this transport in our system therefore restricts cellular access to circulating trehalose rather than reducing its production.

A comparable haemolymph accumulation phenotype has been observed in aphids, where trehalase silencing leads to elevated circulating trehalose due to impaired hydrolysis[26]. In our system, we directly tested this axis by silencing both TreT and TreH in male *A. stephensi*. Reduction of TreH expression similarly increased haemolymph trehalose, confirming that disruption of trehalose hydrolysis elevates circulating levels. Notably, TreT silencing also produced haemolymph accumulation, despite targeting transport rather than enzymatic cleavage. The parallel increase observed under both manipulations indicates that haemolymph trehalose concentration reflects the integrated balance of export, transport, and hydrolysis rather than synthesis alone. Evidence from lepidopterans further supports this interpretation, as disruption of trehalose metabolism depletes systemic energy metabolites even when

trehalose is present [22].These findings reinforce the principle that metabolic stability depends on trehalose flux through the pathway rather than on absolute trehalose abundance in circulation.

Our findings also differ in timing from those reported in *Anopheles gambiae*[27], where TreT silencing produced altered trehalose dynamics after a longer post-injection interval. In that study, haemolymph measurements were performed several days after silencing, allowing additional time for systemic metabolic adjustment. In our experiments, trehalose was quantified 48 h post-injection to coincide with the behavioural window required for mating assays. It is therefore plausible that impaired tissue uptake initially produces haemolymph accumulation, whereas longer-term redistribution or compensatory metabolic shifts may alter circulating levels at later stages. Because reproductive performance declines with mosquito age, extending the post-injection interval was not compatible with accurate mating assessment. The difference in temporal resolution likely accounts for the variation in observed trehalose dynamics rather than indicating mechanistic inconsistency.

Crucially, elevated haemolymph trehalose did not rescue reproductive performance. Females mated with TreT-silenced males produced approximately 20–22% fewer eggs, and combined TreT–TreH silencing amplified this reduction to over 30%. Although the magnitude of reduction following TreT silencing alone may appear moderate, the effect was consistent across three paired replicates and reached statistical significance with a substantial effect size. Importantly, egg production represents a secondary readout of male physiological state, measured indirectly through female output under standardized blood-feeding and oviposition conditions. The absence of differences in unlaid eggs further indicates that female oviposition capacity remained intact, implicating male performance as the limiting factor. These results demonstrate that increased circulating trehalose does not equate to increased functional energy availability. Instead, reproductive success depends on effective trehalose flux from haemolymph into metabolically active tissues.

This causal relationship integrates directly with the stage-specific model established earlier, during which active swarming, trehalase expression peaks, supporting rapid hydrolysis for flight [6]. At coupling, TreT expression increases in fat body, and circulating trehalose rises, indicating redistribution across tissues. When transport capacity is experimentally reduced, trehalose accumulates in circulation but likely cannot be delivered efficiently to tissues during the critical swarm–copulation transition. Even partial disruption of this flux is sufficient to produce measurable downstream consequences in reproductive output. The resulting mismatch between circulating reserve and cellular access likely constrains energy availability during mating behaviours, culminating in reduced egg production.

Collectively, these findings position trehalose transport not merely as a housekeeping function of sugar metabolism but as a rate-limiting step in the coupling of male flight energetics to reproductive success (Fig. 7). By demonstrating that stage-specific redistribution of trehalose across the swarm–mating sequence is both dynamically regulated and functionally consequential, this work identifies TreT-mediated flux as a potential point of physiological vulnerability in male *Anopheles stephensi*. Whether this vulnerability can be exploited through targeted disruption of trehalose transport; either genetically or

through dietary intervention, remains an open question. But the sensitivity of reproductive output to even modest perturbations in transport capacity suggests that such strategies warrant further investigation in the context of vector control.

Limitations

A key limitation of this study is that swarming behaviour could not be directly assessed following gene silencing. Swarm formation in *Anopheles stephensi* requires large numbers of males, and achieving consistent dsRNA-mediated silencing at the population scale necessary for swarming assays was not technically feasible. Consequently, the effects of TreT and TreH disruption on swarm initiation, maintenance, or mating success within natural swarm contexts could not be evaluated. In addition, knockdown efficiency, particularly in the double-silencing experiments, was partial and variable across targets and tissues, which may underestimate the full contribution of trehalose transport and hydrolysis to male reproductive function. Haemolymph carbohydrate measurements were limited to discrete time points and do not capture rapid metabolic dynamics during swarming or copulation. Finally, male reproductive performance was inferred from female egg output, which does not resolve potential effects on sperm transfer efficiency, seminal factors, or female post-mating physiological responses.

Methods

1-In-silico characterisation and phylogenetic analysis of TRET1

The full-length protein sequence of the putative trehalose transporter TRET1 (ASTE010234; 842 aa) was retrieved from VectorBase [28] and submitted to the NCBI Conserved Domain Database (CDD) to identify conserved functional domains(Supplementary Figure S1). The amino acid boundaries of the identified Major Facilitator Superfamily (MFS) domain were recorded and subsequently highlighted on the AlphaFold2 [29] -predicted three-dimensional structure to illustrate the characteristic 12-transmembrane-helix fold. The linear domain architecture was visualised using R [30] and ggplot2 (Fig. 1a, 1a-ii). For phylogenetic analysis, orthologous trehalose transporter sequences were identified by BLASTp searching the MFS domain of ASTE010234 against the VectorBase protein database. Representative sequences from Anophelinae, Culicinae, Chironominae, Brachycera, and an outgroup (Apis mellifera; Hymenoptera) were aligned using MAFFT, and a maximum-likelihood tree was inferred in R using the phangorn and ape packages with 100 bootstrap replicates (supplementary Table S6). The resulting tree was visualised with the Interactive Tree of Life (iTOL) [31], and taxonomic icons were added using BioRender (Fig. 1c).

2-Mosquito Rearing and Maintenance

Anopheles stephensi were maintained following the standard rearing procedures routinely used in our insectary. Mosquitoes were kept at 26–28°C with 70–80% relative humidity under a 12:12 h light: dark cycle. Eggs were placed on the surface of deionized water for hatching, and larvae were reared in iron

trays (66 cm × 45 cm × 17 cm) at a density of approximately 1000 larvae per tray. The larval diet consisted of a 1:1 mixture of powdered dog food (Pet Lover's Crunch Milk Biscuit, India) and fish food (Gold Tokyo, India), provided once daily. Pupae were collected using a plastic dropper and transferred to emergence cages. Newly emerged adults were supplied with sterile 10% sugar solution on cotton pads. For routine colony propagation, females were offered a rabbit blood meal to maintain regular gonotropic cycles.

3-Sugar Diet Preparation and Verification of Feeding Uptake

To confirm ingestion of each sugar treatment, food dyes were incorporated into the solutions prior to feeding. Male and female mosquitoes were provided dyed 10% solutions of erythritol, xylitol, trehalose, and sucrose, or water containing dye as a negative control. A white paper lining was placed at the base of each cage to detect coloured droplets produced through diuresis(Supplementary Figure S2). After 24 hours of exposure, mosquitoes were examined under a stereomicroscope to verify the presence of dye within the body cavity and in dissected midguts, confirming successful ingestion before initiating survival assays.

4-Dietary sugar longevity assay

General methods -Newly eclosed Anopheles stephensi adults were sexed within 24 hours of emergence under cold anaesthesia and transferred into single-sex holding cages. Mosquitoes were provided ad libitum access to one of the following sugar solutions delivered via cotton-wick feeders: 10% sucrose (w/v), serving as the nutritive control, or trehalose, erythritol, or xylitol at concentrations of 2%, 5%, and 10% (w/v). Each treatment comprised 50 mosquitoes per cage, replicated across three independent biological replicates per sex, yielding a total of 150 individuals per treatment per sex. Cages were maintained under standard insectary conditions (27 ± 1°C, 75 ± 5% relative humidity, 12:12 h light:dark photoperiod). Sugar solutions were freshly prepared and cotton wicks replaced every 48 hours to prevent microbial contamination and ensure consistent nutrient delivery. Mortality was recorded daily at a fixed time by counting and removing dead individuals until the last mosquito in each cage had died. No censoring events occurred during the experimental period.

Biostatistical analysis - (Supplementary Table S1) Survival data were analysed using IBM SPSS Statistics (27.0; IBM Corp., Armonk, NY)[32]. Individual survival times (days from eclosion to death) were recorded for each mosquito across all replicates. Biological replicates within each treatment and sex were pooled prior to analysis to generate treatment- and sex-specific survival profiles. Kaplan–Meier survival estimates were computed for each group, and survival curves were plotted as the cumulative proportion surviving against time in days. Mean longevity with 95% confidence intervals was derived from the Kaplan–Meier estimator using the SPSS Life Tables procedure (Analyse → Survival → Kaplan–Meier). Pairwise comparisons between each treatment group and the sucrose control were performed using the log-rank (Mantel–Cox) test, which assigns equal weight to all time points and is appropriate for detecting overall differences in survival distributions. Where multiple pairwise comparisons were conducted within a given sex, the Bonferroni correction was applied to control the family-wise error rate.

In addition, the Breslow (generalised Wilcoxon) test was used as a supplementary comparison to assess whether early divergence in survival curves — particularly relevant for the rapidly lethal erythritol treatments — was consistent with the log-rank results. Significance was set at $\alpha = 0.05$, with adjusted thresholds applied where multiple comparisons were performed. Results are reported as: ns, not significant; *$p < 0.05$; **$p < 0.01$; ***$p < 0.001$. All survival curves and bar charts depicting mean longevity were generated using R (version 4.5.2) with the ggplot2 and survival packages; statistical testing was performed exclusively in SPSS.

5-Mating-status longevity assay

General methods -To evaluate whether reproductive status independently influenced adult lifespan, virgin and mated mosquitoes of both sexes were maintained on 10% sucrose (w/v) under identical rearing conditions as described for the dietary assay. Pupae were sorted by sex under a stereomicroscope based on terminalia morphology and transferred into separate emergence cages (40 × 30 × 40 cm) containing shallow dishes of deionized water to maintain virgin individuals. Newly emerged adults were inspected again to verify that males and females remained correctly separated. For the generation of mated cohorts, three- to four-day-old virgin females were introduced overnight into cages containing an equal number of age-matched virgin males (100 males and 100 females per cage). The following morning, mating success was confirmed by dissecting a random subset of co-housed females (n = 4–5) and examining the spermathecae for the presence of motile sperm under a light microscope. Males from cages in which spermathecal confirmation was positive were considered to have mated successfully. Successfully mated males and females were then separated and transferred into single-sex cages (n = 50 per group, three biological replicates per sex). Age-matched virgin controls of both sexes were maintained in parallel cages without prior exposure to the opposite sex. Mating partners were sugar-fed individuals of the opposite sex, designated SF female (for male mated cohorts) and SF male (for female mated cohorts). Sugar solutions and cotton wicks were replaced every 48 hours. Mortality was recorded daily at a fixed time until the death of the last individual in each cage. No censoring events occurred.

Biostatistical analysis (Supplementary Table S2.) - Survival data from the mating-status assay were analysed using IBM SPSS Statistics (version 27.0; IBM Corp., Armonk, NY) following the same framework as described for the dietary assay. Individual survival times for virgin and mated cohorts were pooled across biological replicates within each sex. Kaplan–Meier survival estimates were computed separately for virgin males, mated males, virgin females, and mated females using the SPSS Kaplan–Meier procedure (Analyse → Survival → Kaplan–Meier), with mating status defined as the factor variable and survival time in days as the time variable. Mean longevity with 95% confidence intervals was extracted from the Kaplan–Meier output for each group (Supplementary Figure S3). Statistical comparison between virgin and mated cohorts within each sex was performed using the log-rank (Mantel–Cox) test as the primary inferential test. Given that only a single pairwise comparison was made within each sex (virgin versus mated), no correction for multiple comparisons was required. The Breslow (generalised Wilcoxon) and Tarone–Ware tests were additionally performed to confirm the

robustness of the results across tests that differentially weight early, middle, and late survival events, respectively. Effect size was reported as the difference in mean longevity between virgin and mated groups, expressed both in absolute days and as a percentage reduction relative to the virgin cohort. Significance was set at $\alpha = 0.05$, with results reported as: ***$p < 0.001$; ****$p < 0.0001$. All figures were generated in R (version 4.5.2) using the ggplot2 and survival packages; statistical analyses were conducted exclusively in SPSS.

6-Mating-sequence Classification and Sample Collection

Mating stages were identified through direct behavioural observation in standard mesh cages. Adult males and females (3–4 days' post-emergence) were introduced into a common cage at 3:00 PM, and samples were collected at defined time points representing distinct mating states. Control males were collected at 12:00 PM before exposure to females. Pre-swarm males were sampled at 6:00 PM on the same day of mixing, prior to the onset of swarm formation. Active-swarm males were collected between 7:00 and 8:00 PM, during the period of peak circular flight characteristic of swarm behaviour. Coupled individuals – male and female pairs engaged in copulation (Supplementary Table S6), were aspirated directly from the swarm during the same time window, with the collection procedure documented in Supplementary Video. Post-swarm males were collected at 7:00 AM the following morning, after swarm activity had ceased, representing the recovery phase(Supplementary Table S3).

7-Tissue Dissection, RNA Extraction, cDNA Synthesis, and Quantitative PCR

General methods - Fat body and midgut tissues were dissected from adult males under a stereomicroscope in ice-cold, DEPC-treated nuclease-free water to minimise RNA degradation. Dissections were performed immediately following each behavioural stage (control, pre-swarm, active swarm, coupled, and post-swarm), and tissues were transferred to RNase-free microcentrifuge tubes, flash-frozen on dry ice, and stored at − 80°C until RNA isolation. Total RNA was extracted using TRIzol reagent (Invitrogen) according to the manufacturer's protocol. RNA concentration and purity were assessed by absorbance at 260/280 nm using a NanoDrop spectrophotometer (Thermo Scientific); samples with A260/280 ratios between 1.8 and 2.1 were accepted for downstream processing. Approximately 1 µg of total RNA per sample was reverse-transcribed into first-strand cDNA using a mixture of oligo(dT) and random hexamer primers with the Verso cDNA Synthesis Kit (Cat# AB-1453/A, Thermo Scientific, Lithuania). An on-column DNase treatment step was included to eliminate residual genomic DNA contamination. cDNA was diluted to a working concentration and stored at − 20°C until use. Transcript integrity was routinely verified by conventional RT-PCR using gene-specific primers (Supplementary Table 4) followed by agarose gel electrophoresis prior to quantitative analysis.

Quantitative PCR was performed using SYBR Green qPCR Master Mix (Thermo Scientific) on a CFX96 Real-Time PCR Detection System (Bio-Rad, USA). The thermal cycling protocol consisted of an initial denaturation at 95°C for 15 min, followed by 40 cycles of 95°C for 10 s, 52°C for 15 s, and 72°C for 22 s. A melt-curve analysis (65–95°C, 0.5°C increments) was appended to each run to verify amplification specificity and the absence of primer dimers (Supplementary Table S4, Supplementary Figure S4). Each

experimental condition was represented by three independent biological replicates, with two technical replicates per biological replicate per target gene.

Biostatistical analysis - Expression of the trehalose transporter (Tret1) and trehalase (Treh) was quantified in midgut and fat body tissues across five behaviourally defined mating stages: control (non-swarming), pre-swarm, active swarm, coupled, and post-swarm. Technical replicate Cq values were averaged for each biological replicate prior to analysis. Expression was normalised to the geometric mean of the Cq values of two internal reference genes, Actin and S7 (calculated as √[Actin × S7]), to provide a multiplicative correction that accounts for the wider dynamic range of reference gene expression observed across tissue types. The 2^−ΔΔCt method was applied with the within-tissue control stage serving as the calibrator, such that each tissue was independently normalised to its own baseline. This design permitted direct comparison of expression dynamics across mating stages within each tissue without confounding by tissue-level differences in absolute transcript abundance.

Statistical comparisons between specific mating stages were performed using paired Student's t-tests conducted on ΔCt values rather than on fold-change values. The paired design was selected because the same biological replicates (matched by dissection batch and RNA extraction date) were measured across all mating stages, and pairing removes inter-replicate variability that would otherwise inflate the error term. Testing was performed on the ΔCt scale rather than the 2^−ΔΔCt scale because ΔCt values are log-transformed expression ratios that conform more closely to a normal distribution, thereby satisfying the assumptions of the parametric t-test; fold-change values, by contrast, are exponentially distributed and prone to skew, which can compromise the validity of parametric inference at small sample sizes. Relative gene expression was calculated using the 2^−ΔΔCt method [33]. Pairwise t-tests were conducted between all mating-stage groups within each tissue for both Trehalose transporter and Trehalase; only comparisons that reached statistical significance are displayed in the figure (figure – 3) for clarity. P-values less than 0.05 were considered significant and denoted with an asterisk; non-significant results retained in the figures were labelled "ns." Bar plots depict mean relative expression ± SEM; trend line plots show mean expression with shaded SEM ribbons across mating stages. All RT-qPCR data processing, statistical analyses, and visualisations were performed in R (version 4.5.2) using the tidyverse (v2.0.0), ggplot2, and ggpubr packages.

8-Haemolymph Collection and Trehalose Quantification

General methods. Haemolymph was collected from adult males at each of the five behaviourally defined mating stages (control, pre-swarm, active swarm, coupled, and post-swarm) by gently piercing the lateral thorax with a fine glass capillary needle and drawing exuding droplets directly into calibrated glass capillaries. Haemolymph from 20 mosquitoes was pooled per biological replicate to obtain sufficient volume for enzymatic analysis. Three independent biological replicates were collected per mating stage. Samples were immediately transferred to chilled, RNase-free microcentrifuge tubes, kept on ice throughout handling, and stored at − 80°C until assayed.

Trehalose and glucose concentrations were quantified using the Megazyme Trehalose Assay Kit (K-TREH, Megazyme, Ireland), following the microplate procedure described in the manufacturer's instructions. The assay exploits a two-step enzymatic cascade: haemolymph samples are first incubated to measure endogenous free glucose, and then treated with exogenous trehalase to hydrolyse trehalose into its glucose constituents. The resulting glucose is phosphorylated to glucose-6-phosphate by hexokinase and subsequently oxidised by glucose-6-phosphate dehydrogenase, generating NADPH in stoichiometric proportion to glucose content. Absorbance was measured at 340 nm using a microplate reader at two time points: an initial reading after a 5-minute incubation to quantify baseline free glucose (A1), and a second reading following addition of trehalase and a further 5-minute incubation to quantify total glucose including trehalose-derived glucose (A2). All samples were assayed in technical duplicates and analysed within the linear range of the enzymatic reaction [34].

Standard curve generation and data processing- A glucose standard curve was prepared independently for each assay plate using serial dilutions of the D-glucose standard supplied with the Megazyme kit. Standards were run in duplicate across a concentration range covering the expected haemolymph values. Absorbance values were fitted to a linear regression model (concentration as a function of absorbance). Each biological replicate was calibrated against its own plate-matched standard curve ($R^2 \geq 0.99$). Endogenous free glucose concentration was calculated by converting the baseline absorbance reading (A1) to glucose mass equivalents (µg) using the replicate-specific regression equation, dividing by the molecular weight of glucose (180.16 g/mol), and normalising to the sample volume (20 µL) to express final values in millimolar (mM). Trehalose-derived glucose concentration was calculated by converting the post-trehalase absorbance (A2) to mass equivalents, subtracting the baseline glucose mass to isolate the trehalose-specific signal, dividing by the molecular weight of trehalose (342.30 g/mol), and normalising to the same sample volume to express values in mM. The trehalose-to-glucose ratio was computed for each sample as the quotient of trehalose concentration over glucose concentration, providing a measure of the relative composition of the circulating carbohydrate pool at each mating stage. For stacked composition analysis, the percentage contribution of trehalose and glucose to the total carbohydrate pool was calculated by expressing each metabolite as a proportion of the combined trehalose-plus-glucose concentration.

Biostatistical analysis -Statistical comparisons of haemolymph metabolite concentrations across mating stages were performed using linear mixed-effects models (LMMs) fitted with the lme4 and lmerTest packages in R (version 4.5.2). LMMs were selected because the experimental design involved repeated measurements across mating stages within each of three biological replicates, introducing a hierarchical correlation structure that violates the independence assumption of standard ANOVA or t-tests. Observations from the same biological replicate - which share a common haemolymph pool, extraction batch, and plate calibration ,are inherently correlated, and treating them as independent would inflate the effective sample size and produce artificially narrow confidence intervals. The LMM addresses this by modelling biological replicate as a random intercept (model: Concentration_mM ~ Stage + (1 | Replicate)), which partitions the total variance into a between-replicate component

(absorbed by the random effect) and a within-replicate, between-stage component (estimated as the fixed effect of interest).

For the trehalose-to-glucose ratio, an LMM with Stage as the fixed effect and Replicate as a random intercept was fitted across all five mating stages, with each non-control stage compared to the control baseline using the model coefficients. For individual carbohydrate pool comparisons (glucose and trehalose separately), pairwise LMMs were fitted between control and each mating stage of interest. Where the direction of change was biologically predicted ; specifically, that trehalose concentration would decrease following the energetically demanding swarm–mating sequence — one-tailed p-values were derived by halving the two-tailed p-value from the model output. For comparisons without a directional prediction (e.g., glucose between control and post-swarm), two-tailed p-values were reported. The Satterthwaite approximation for degrees of freedom was used throughout, as it provides a more conservative estimate of denominator degrees of freedom than the default Wald test when the number of random-effect groups is small. Significance was set at $\alpha = 0.05$, with results reported as: ns, not significant; *$p < 0.05$; **$p < 0.01$; ***$p < 0.001$. All trehalose data processing, statistical modelling, and visualisations were performed in R (version 4.5.2) using the tidyverse, ggplot2, stringr, lme4, and lmerTest packages.

9-dsRNA Synthesis and Gene Silencing (RNAi)

General methods - Double-stranded RNA (dsRNA) targeting the trehalose transporter gene (TreT) was synthesised using gene-specific primers carrying T7 promoter overhangs at both positions (Supplementary Table S5). PCR amplicons were verified on 1.5% agarose gels, purified (GeneJET PCR Purification Kit, Thermo Scientific), and used as templates for in vitro transcription (TranscriptAid T7 High-Yield Transcription Kit, Ambion, USA). Following DNase I treatment, dsRNA was annealed by slow cooling from 95°C to room temperature, purified by ethanol precipitation, verified on agarose gels, and adjusted to 3 µg/µL in nuclease-free water. A non-target dsGFP fragment with no homology to the An. stephensi genome served as the injection control. For the double-knockdown experiment, dsRNA targeting both TreT and TreH was co-injected at equimolar concentrations.

Male mosquitoes (0–1 days post-eclosion) were cold-anaesthetised and microinjected in the lateral thorax with approximately 69 nL of dsRNA solution (~ 207 ng per mosquito) using a Nanoject III nano-injector (Drummond Scientific, USA). Age-matched dsGFP-injected males served as controls for each biological replicate. Injected mosquitoes were maintained under standard insectary conditions (27 ± 1°C, 75 ± 5% RH, 12:12 h L:D) with 10% sucrose ad libitum. Individuals that died within 24 hours were excluded as injection-related losses. At 48 hours post-injection, knockdown efficiency was validated by RT-qPCR on dissected fat body and whole-body tissues using the same extraction, cDNA synthesis, and qPCR protocols described for the mating-stage expression profiling, with two technical replicates per biological replicate. Unlike the mating-stage experiment, where expression was normalised to the geometric mean of Actin and S7, knockdown samples were normalised to S7 alone, as dsRNA-mediated silencing introduced instability in Actin amplification across treatment groups.

Biostatistical analysis

(i) Initial knockdown validation (whole-body TH and fat body TT). Knockdown efficiency of TH in whole body and TT in fat body was assessed in dsRNA-injected versus dsGFP-injected mosquitoes across three biological replicates. Expression was normalised to S7 using the 2^−ΔCq method (ΔCq = Cq_target − Cq_S7), without a ΔΔCt calibration step, as the comparison required only relative quantification between two groups. Normalised expression values (2^−ΔCq) were compared between control and silenced groups using unpaired Welch's t-tests. The Welch correction was selected because dsRNA-mediated silencing typically introduces heterogeneous knockdown penetrance across individuals, resulting in unequal variance between groups that would violate the assumptions of the classical Student's t-test. Percentage reduction in expression was calculated as [(mean_control − mean_silenced) / mean_control] × 100 and reported alongside p-values.
(ii) Expanded fat body TT knockdown validation. A second, independent knockdown experiment was performed to confirm TT silencing in the fat body using four biological replicates. In this experiment, S7 exhibited greater inter-replicate variability than Actin in fat body samples; expression was therefore normalised to Actin alone using the 2^−ΔCq method. The choice of reference gene was determined empirically for each experiment based on which reference showed the lowest coefficient of variation across samples, consistent with recommended practice for qPCR normalisation. A fixed-effects linear model was fitted to ΔCq values with knockdown status and biological replicate as independent variables (ΔCq ~ Status + BioRep). Inclusion of BioRep as a covariate absorbs batch-to-batch variation, isolating the treatment effect with greater precision than an unpaired test. The two-tailed p-value for the Status coefficient was halved to yield a one-tailed p-value, reflecting the directional hypothesis that dsRNA injection reduces target transcript abundance, given that the RNAi mechanism is unidirectional. Technical replicates were averaged prior to plotting, and results are presented as mean normalised expression ± standard deviation with individual data points overlaid. All knockdown validation analyses were performed in R (version 4.5.2) using the tidyverse (v2.0.0), ggplot2, and ggpubr packages.

10-Haemolymph Trehalose Quantification Following Gene Silencing

To assess the effect of gene silencing on circulating trehalose levels, haemolymph was collected at 48 h post-injection from dsGFP-injected (control), dsTreT-silenced, and dsTreH-silenced males following the same pooling and storage protocol described for the mating-stage assay (20 mosquitoes per pool, three biological replicates per group). Trehalose was quantified using the Megazyme Trehalose Assay Kit as described above. The validated regression slope derived from the mating-stage standard curves was applied to convert absorbance to concentration, maintaining calibration consistency across experiments. For each sample, technical replicate absorbance values were averaged at each time point, and the change in absorbance relative to the pre-trehalase baseline (ΔA) was converted to trehalose concentration (µg/well). Mean concentration was calculated across all plateau-phase time points (5–40 min at 5-minute intervals) per replicate per treatment group to capture the full equilibrium phase rather than relying on a single endpoint. Trehalose concentrations were compared across treatment groups using an LMM (Trehalose_conc ~ Stage + (1 | bio_rep)), with each silenced group compared to the

dsGFP control using the fixed-effect coefficients. Statistical parameters (Satterthwaite degrees of freedom, significance thresholds) were as described for the mating-stage analysis.

11-Egg-laying Assay (Fecundity)

General methods- To assess post-mating reproductive output, virgin females aged 3–4 days were paired overnight with either dsGFP-injected (control) or gene-silenced males at a 1:1 ratio in standard mesh cages. The following morning, mated females were blood fed on a rabbit. Only fully engorged females were retained for the assay; partially or incompletely blood-fed individuals were removed to ensure uniform vitellogenic development. Engorged females were maintained under standard insectary conditions for 48 hours to allow completion of the gonotrophic cycle and full egg maturation.

For oviposition, 20 fully engorged females from each treatment group were transferred individually into netted plastic cups (10 cm diameter × 5.75 cm depth) containing one-third volume of deionised water and lined with filter paper as an egg-laying substrate. After a 24-hour oviposition period, filter papers were removed, air-dried, and examined under a stereomicroscope for egg counting. Each female's total egg output was recorded as the sum of eggs successfully laid on the substrate plus any eggs retained within the reproductive tract (determined by dissection of post-oviposition females). For single gene knockdowns (dsTreT alone), fecundity assays were performed across three independent biological replicates. For double knockdowns (dsTreT + dsTreH), the assay was conducted across three biological replicates with unequal replicate sizes due to experimental constraints.

Biostatistical analysis - Egg count data were analysed using Welch's two-sample t-tests, which do not assume equal variances between treatment groups and automatically adjust for unequal sample sizes when present. The Welch correction was selected because gene silencing treatments can introduce heterogeneous effects across individual females, leading to different variances between control and silenced groups that would violate the assumptions of the classical Student's t-test. Total egg production (laid plus unlaid eggs combined) served as the primary outcome variable, as this metric captures the full reproductive output irrespective of oviposition behaviour. Effect size was quantified using Cohen's d with Hedges' correction for unequal variances, calculated as the standardised difference between group means. The percentage reduction in fecundity was calculated as [(mean_control − mean_silenced) / mean_control] × 100. For visualisation, data were presented as violin plots with embedded box plots and individual data points (jittered to avoid overplotting), with group means indicated by coloured diamond markers. Statistical significance brackets were added using the ggpubr package, with p-values reported as: ns, not significant; *p < 0.05; **p < 0.01; ***p < 0.001; ****p < 0.0001. All fecundity data processing, statistical analyses, and visualisations were performed in R (version 4.5.2) using the tidyverse, ggplot2, ggpubr, and rstatix packages.

Declarations

Data Availability Statement

All data supporting the findings of this study are available within the article and its supplementary materials. Raw data files, reproducible RMarkdown analysis scripts, trehalose assay data, sequence alignments, maximum-likelihood tree files, and video documentation of mating behaviour have been deposited in Figshare and are accessible at *https://doi.org/10.6084/m9.figshare.31648699.* The Anopheles stephensi trehalose transporter sequence (ASTE010234) is available through VectorBase (https://vectorbase.org)

Author Contributions

Conceptualization: N.S., T.S., R.D.; Data curation: N.S., T.S.; Formal analysis: N.S., T.S.; Investigation: N.S., T.S., P.Y., V.S., P.R., V.Sr., G.S., P.S.; Methodology: N.S., T.S., P.S., R.D.; Project administration: R.D.; Resources: R.D.; Supervision: R.D., P.S., S.T.; Validation: N.S., T.S.; Visualization: T.S.; Writing – original draft: T.S., N.S.; Writing – review & editing: N.S., T.S., P.S., S.T., R.D., S.Tev.

Author initials used:

N.S. (Nirmala Sankhala), T.S. (Tanvi Singh), P.Y. (Pooja Yadav), V.S. (Vaishali Saini), P.R. (Pooja Rohilla), V.Sr. (Vartika Srivastava), G.S. (Gunjan Sharma), S.T. (Suchi Tyagi), S.Tev. (Sanjay Tevatiya), P.S. (Punita Sharma), R.D. (Rajnikant Dixit).

Additional Information

Ethics Declaration

All experimental protocols involving the use of live rabbits for mosquito blood-feeding were approved by the Institutional Animal Ethics Committee, ICMR-National Institute of Malaria Research (NIMR/IAEC/2022-1/08; dated 20 April 2022), registered under CPCSEA (Registration No. 33/GO/ReBi/S/99/CPCSEA). All methods were carried out in accordance with relevant guidelines and regulations. Rabbits used for blood-feeding were obtained from the Laboratory Animal Resources Section, Division of Animal Genetics, ICAR-Indian Veterinary Research Institute, Izatnagar, Bareilly, Uttar Pradesh, India. *Anopheles stephensi* mosquitoes were maintained at the Central Insectary Facility, ICMR-National Institute of Malaria Research, Dwarka, New Delhi.

Acknowledgment: We would like to thank the ICMR-National Institute of Malaria Research

insectary staff members for mosquito rearing. We thank Kunwarjeet Singh, Sattey Singh,

Lipun and Nishant for their technical assistance in the laboratory.

Funding: Laboratory work was supported by the ICMR Grant (Ref # VBD/NIMR/Intra/002- ECD-II). Nirmala is the recipient of UGC fellowship (Ref # 191620022266). The funders had no role in study design, data collection and analysis, decision to publish, or preparation of the manuscript.

References

1. Subbarao, S. K., Nanda, N., Rahi, M. & Raghavendra, K. Biology and bionomics of malaria vectors in India: existing information and what more needs to be known for strategizing elimination of malaria. *Malar. J.* **18**, 396–396 (2019).
2. Attardo, G. M., Hansen, I. A. & Raikhel, A. S. Nutritional regulation of vitellogenesis in mosquitoes: Implications for anautogeny. *Insect Biochem. Mol. Biol.* **35**, 661–675 (2005).
3. Foster, W. A. Mosquito Sugar Feeding and Reproductive Energetics. *Annu. Rev. Entomol.* **40**, 443–474 (1995).
4. Huck, D. T., Klein, M. S. & Meuti, M. E. Determining the effects of nutrition on the reproductive physiology of male mosquitoes. *J. Insect Physiol.* **129**, (2021).
5. Gary, R. E., Cannon, J. W. & Foster, W. A. Effect of sugar on male Anopheles gambiae mating performance, as modified by temperature, space, and body size. *Parasit. Vectors* **2**, 19–19 (2009).
6. YUVAL, B., HOLLIDAY-HANSON, M. L. & WASHING, R. K. Energy budget of swarming male mosquitoes. *Ecol. Entomol.* **19**, 74–78 (1994).
7. Kikawada, T. *et al.* Trehalose transporter 1, a facilitated and high-capacity trehalose transporter, allows exogenous trehalose uptake into cells. *Proc. Natl. Acad. Sci.* **104**, 11585–11590 (2007).
8. Tevatiya, S. *et al.* Molecular and Functional Characterization of Trehalase in the Mosquito Anopheles stephensi. *Front. Physiol.* **11**, (2020).
9. Becker, A., Schlöder, P., Steele, J. E. & Wegener, G. The regulation of trehalose metabolism in insects. *Experientia* **52**, 433–439 (1996).
10. Tellis, M. B. *et al.* Trehalose transporter-like gene diversity and dynamics enhances stress response and recovery in Helicoverpa armigera. *Gene* **862**, 147259–147259 (2023).
11. Cavagna, A. *et al.* Characterization of lab-based swarms of Anopheles gambiae mosquitoes using 3D-video tracking. *Sci. Rep.* **13**, 8745–8745 (2023).
12. Chadee, D. D., Sutherland, J. M. & Gilles, J. R. L. Diel sugar feeding and reproductive behaviours of Aedes aegypti mosquitoes in Trinidad: With implications for mass release of sterile mosquitoes. *Acta Trop.* **132**, S86–S90 (2014).
13. Briegel, H. & Timmermann, S. E. Aedes albopictus (Diptera: Culicidae): Physiological Aspects of Development and Reproduction. *J. Med. Entomol.* **38**, 566–571 (2001).
14. Strampelli, A. *et al.* A male-drive female-sterile system for the self-limited control of the malaria mosquito Anopheles gambiae. *Nat. Commun.* **16**, 9446–9446 (2025).
15. Arnqvist, G., Rönn, J., Watson, C., Goenaga, J. & Immonen, E. Concerted evolution of metabolic rate, economics of mating, ecology, and pace of life across seed beetles. *Proc. Natl. Acad. Sci.* **119**, (2022).
16. Barredo, E. & DeGennaro, M. Not Just from Blood: Mosquito Nutrient Acquisition from Nectar Sources. *Trends Parasitol.* **36**, 473–484 (2020).
17. Elbein, A. D., Pan, Y. T., Pastuszak, I. & Carroll, D. New insights on trehalose: A multifunctional molecule. *Glycobiology* **13**, (2003).

18. Miyamoto, T. & Amrein, H. Gluconeogenesis: An ancient biochemical pathway with a new twist. *Fly (Austin)* **11**, 218–223 (2017).
19. Chaudhari, B. Y., Nichit, V. J., Barvkar, V. T. & Joshi, R. S. Mechanistic insights in the role of trehalose transporter in metabolic homeostasis in response to dietary trehalose. *G3 Genes Genomes Genet.* https://doi.org/10.1093/g3journal/jkaf303 (2025) doi:10.1093/g3journal/jkaf303.
20. Rochlin, I. *et al.* Laboratory evaluation of sugar alcohols for control of mosquitoes and other medically important flies. *Sci. Rep.* **12**, (2022).
21. Matsuda, H., Yamada, T., Yoshida, M. & Nishimura, T. Flies without trehalose. *J. Biol. Chem.* **290**, 1244–1255 (2015).
22. Mohite, S. *et al.* Trehalose metabolism regulates transcriptional control of muscle development in lepidopteran insects. https://doi.org/10.7554/eLife.109485.1 (2026) doi:10.7554/eLife.109485.1.
23. Tian, Z. *et al.* Trehalose metabolism mediates trade-offs between reproduction and survival in beet webworm, Loxostege sticticalis, under heat stress. *Pest Manag. Sci.* **81**, 903–911 (2025).
24. Thompson, S. N. Trehalose - The Insect 'Blood' Sugar. *Adv. Insect Physiol.* **31**, 205–285 (2003).
25. Kanamori, Y. *et al.* The trehalose transporter 1 gene sequence is conserved in insects and encodes proteins with different kinetic properties involved in trehalose import into peripheral tissues. *Insect Biochem. Mol. Biol.* **40**, 30–37 (2010).
26. Wang, G. *et al.* Trehalose and glucose levels regulate feeding behavior of the phloem-feeding insect, the pea aphid Acyrthosiphon pisum Harris. *Sci. Rep.* **11**, (2021).
27. Liu, K., Dong, Y., Huang, Y., Rasgon, J. L. & Agre, P. Impact of trehalose transporter knockdown on Anopheles gambiae stress adaptation and susceptibility to Plasmodium falciparum infection. *Proc. Natl. Acad. Sci.* **110**, 17504–17509 (2013).
28. Giraldo-Calderón, G. I. *et al.* VectorBase: an updated bioinformatics resource for invertebrate vectors and other organisms related with human diseases. *Nucleic Acids Res.* **43**, D707–D713 (2015).
29. Varadi, M. *et al.* AlphaFold Protein Structure Database: massively expanding the structural coverage of protein-sequence space with high-accuracy models. *Nucleic Acids Res.* **50**, D439–D444 (2022).
30. RStudio Team. RStudio: Integrated Development for R. RStudio, Inc., Boston, . https://doi.org/10.59350/t79xt-tf203 doi:10.59350/t79xt-tf203.
31. Letunic, B. itol. https://doi.org/10.1093/nar/gkae268.
32. Morgan, G. A., Barrett, K. C., Leech, N. L. & Gloeckner, G. W. *IBM SPSS for Introductory Statistics: Use and Interpretation*. (Routledge, Sixth edition. | New York, NY : Routledge, 2020., 2019). doi:10.4324/9780429287657.
33. Livak, K. J. & Schmittgen, T. D. Analysis of Relative Gene Expression Data Using Real-Time Quantitative PCR and the 2−ΔΔCT Method. *Methods* **25**, 402–408 (2001).
34. Marten, A. D., Stothard, A. I., Kalera, K., Swarts, B. M. & Conway, M. J. Validamycin A Delays Development and Prevents Flight in Aedes aegypti (Diptera: Culicidae). *J. Med. Entomol.* **57**, 1096–1103 (2020).

Figures

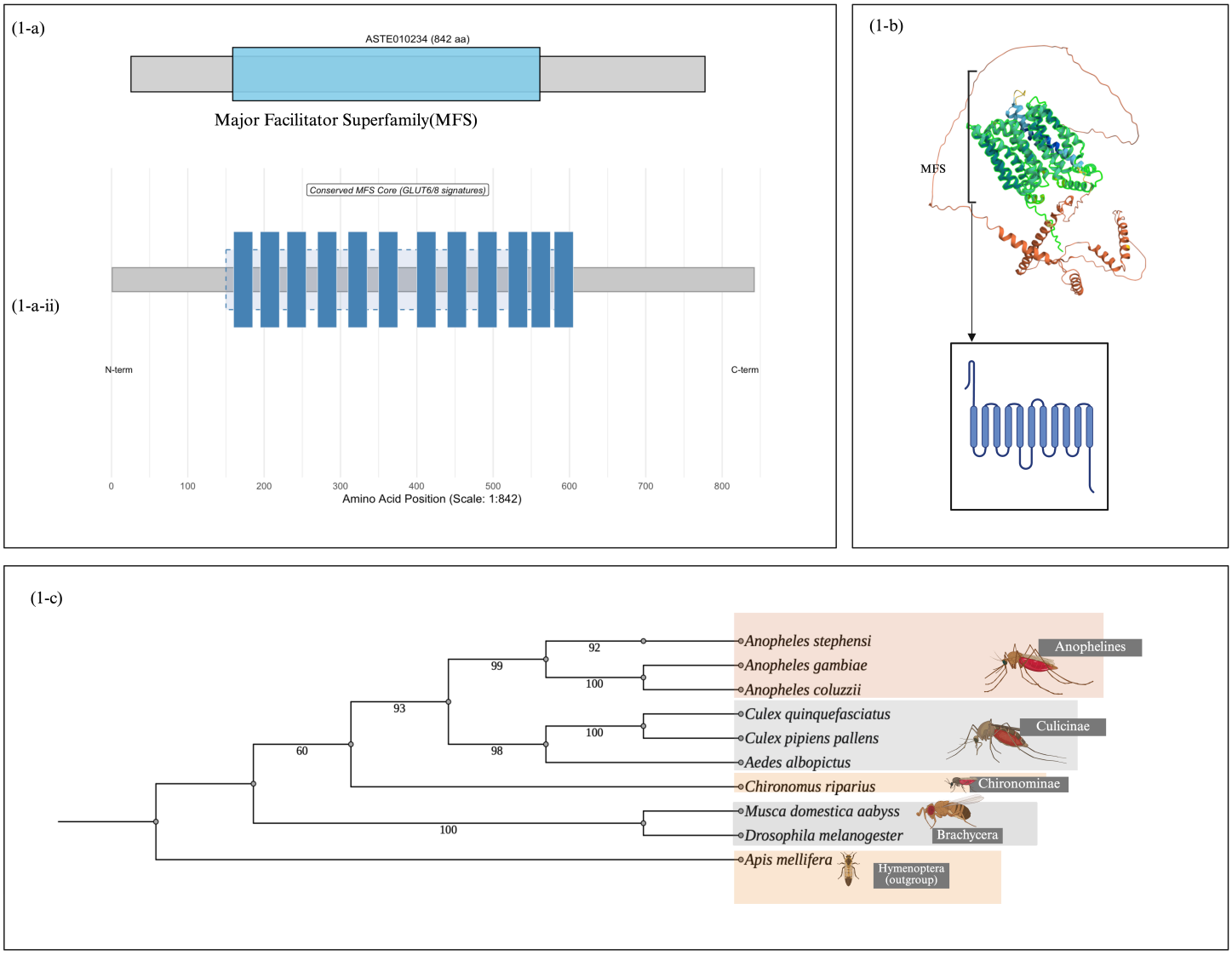


Figure 1

Structural, domain, and evolutionary features of the *Anopheles stephensi* trehalose transporter (TRET1). **(a)** Linear domain architecture of *AsTRET1*(ASTE010234; 842 aa) showing the conserved Major Facilitator Superfamily (MFS) core. The central region contains the canonical 12 predicted transmembrane helices and conserved GLUT6/8-like signature motifs typical of insect trehalose transporters, flanked by extended N- and C-terminal regions. **(b)** AlphaFold2-predicted three-dimensional structure of *AsTRET*1 illustrating the characteristic MFS fold and alternating-access topology of sugar porters; the inset depicts the 12-transmembrane-helix organization underlying facilitated trehalose transport. **(c)** Maximum-likelihood phylogenetic analysis of *AsTRET1* and related insect trehalose transporters, inferred from aligned protein sequences. Node support values represent bootstrap percentages based on 100 replicates. *Anopheles stephensi* clusters robustly with other anopheline

mosquitoes, forming a distinct clade separated from culicine mosquitoes (*Aedes*, *Culex*) and other dipterans, with *Apis mellifera* included as an outgroup.

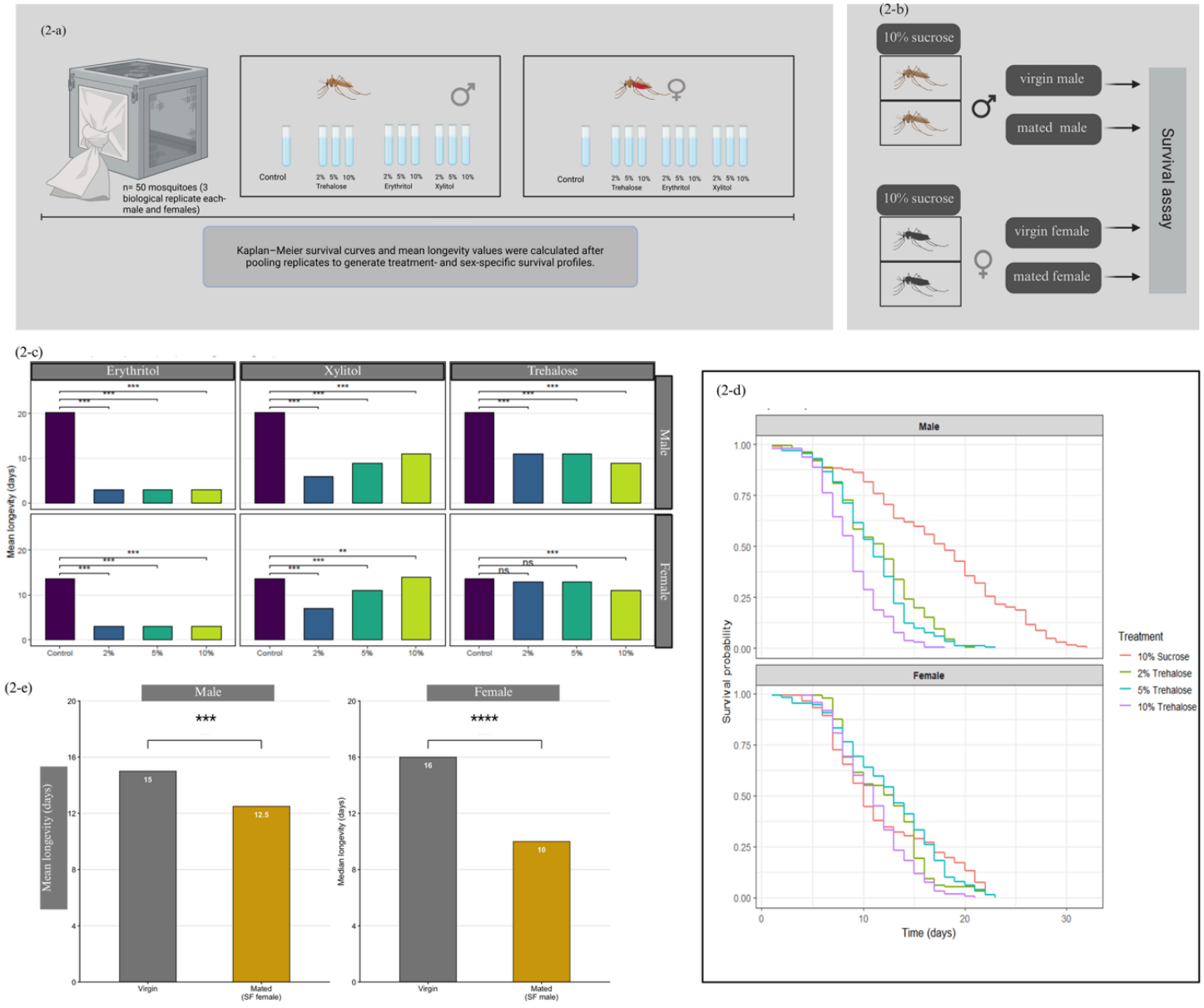


Figure 2

Differential effects of dietary sugars and mating status on adult survival in *Anopheles stephensi*. (a) Schematic overview of the experimental design for dietary longevity assays. Adult males and females were housed separately in cages (n = 50 per treatment, three biological replicates per sex) and provided with sucrose (control), trehalose, erythritol, or xylitol at 2%, 5%, and 10% concentrations. Survival was recorded daily, and replicates were pooled to generate treatment- and sex-specific survival profiles. (b) Experimental design for the mating-status longevity assay. Virgin and mated adults of both sexes were maintained on 10% sucrose and monitored daily. (c) Mean longevity (days) of males (top row) and females (bottom row) fed erythritol, xylitol, or trehalose at indicated concentrations compared with sucrose-fed controls. Bars represent mean lifespan pooled across three biological replicates. Statistical

comparisons were performed using log-rank (Mantel–Cox) tests; ns, not significant; **p < 0.01; ***p < 0.001. (d) Kaplan–Meier survival curves for males (top) and females (bottom) maintained on 10% sucrose (red), 2% trehalose (yellow), 5% trehalose (cyan), and 10% trehalose (purple). Survival probability is plotted as a function of time (days). (e) Mean longevity of virgin versus mated males (left) and females (right) maintained on 10% sucrose. Mating partners were sugar-fed individuals of the opposite sex (SF female and SF male, respectively). Values above bars indicate group means; ***p < 0.001; ****p < 0.0001.

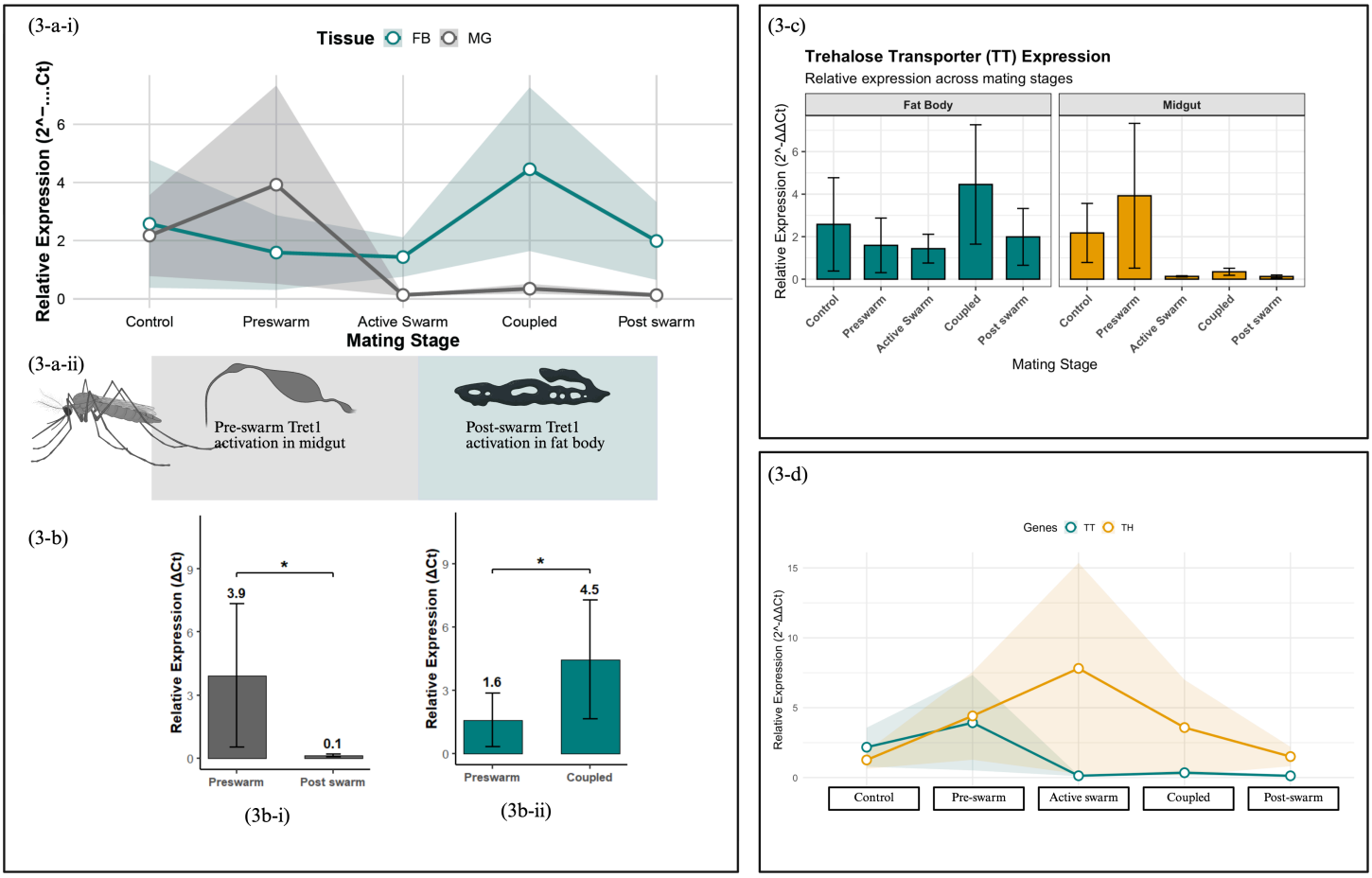


Figure 3

Dynamic regulation of trehalose transporter (TreT) and trehalase expression across the swarm–mating sequence in male *Anopheles stephensi*. (a-i) Relative TreT transcript levels in fat body (FB) and midgut (MG) measured across defined mating stages (Control, Pre-swarm, Active swarm, Coupled, Post-swarm). Expression values are shown as mean with variability across three independent biological replicates, normalized to internal reference genes (Actin and S7). (a-ii) Conceptual schematic summarizing the observed tissue-specific shift in TreT expression, with elevated midgut expression prior to swarm initiation and increased fat-body expression during mating. (b) Pairwise statistical comparisons of TreT expression between selected mating stages. In the midgut, TreT expression was significantly reduced between Pre-swarm and Post-swarmstages (p = 0.045; paired t-test). In the fat

body, TreT expression was significantly higher in Coupled males compared to Pre-swarm males (p = 0.038; paired t-test). Mean expression values are indicated above bars. (c) Stage-wise comparison of TreT expression in fat body and midgut presented as mean ± SEM across biological replicates, illustrating reciprocal tissue-specific regulation across the mating sequence. (d) Comparative expression profiles of TreT and trehalase (TreH) in the midgut across mating stages. Trehalase expression peaks during the Active swarm stage, whereas TreT expression remains comparatively stable, indicating stage-specific regulation of trehalose hydrolysis during swarm activity.

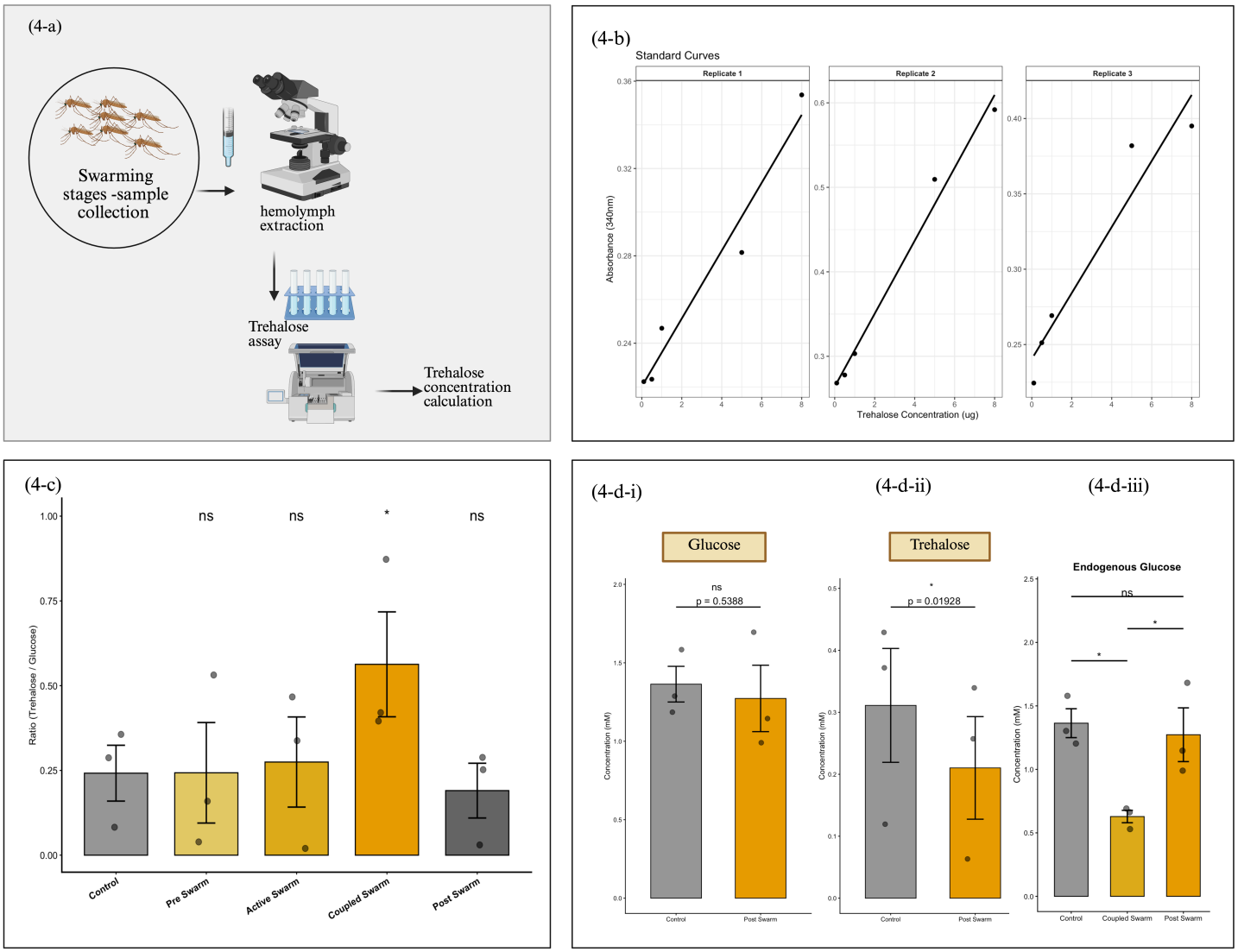


Figure 4

Stage-linked fluctuations in circulating trehalose and glucose during male reproductive activity in *Anopheles stephensi*. (a) Schematic overview of the haemolymph collection and trehalose quantification workflow. Males were sampled at defined swarming and mating stages, haemolymph was extracted, enzymatically processed, and trehalose concentration was quantified using a plate-based assay. (b) Representative standard curves generated for trehalose-derived glucose quantification across three independent biological replicates. Absorbance at 340 nm is plotted against trehalose concentration, and linear regression was used for concentration calculations within the linear range of the assay. (c) Ratio

of trehalose to glucose in haemolymph across mating stages (Control, Pre-swarm, Active swarm, Coupled swarm, Post-swarm). Bars represent mean values across biological replicates with individual data points overlaid. Statistical comparisons were performed relative to the control; ns, not significant; $p < 0.05$. (d) Pairwise comparisons of haemolymph carbohydrate pools were assessed using linear mixed-effects models (LMM). (d-i) Glucose concentrations in Control versus Post-swarm males show no significant difference (ns; $p = 0.5388$). (d-ii) Trehalose concentrations are significantly reduced in Post-swarm males compared to Control ($p = 0.01928$). (d-iii) Endogenous glucose levels across Control, Coupled swarm, and Post-swarmstages, with significant differences indicated ($p < 0.05$) and non-significant comparisons marked as ns.

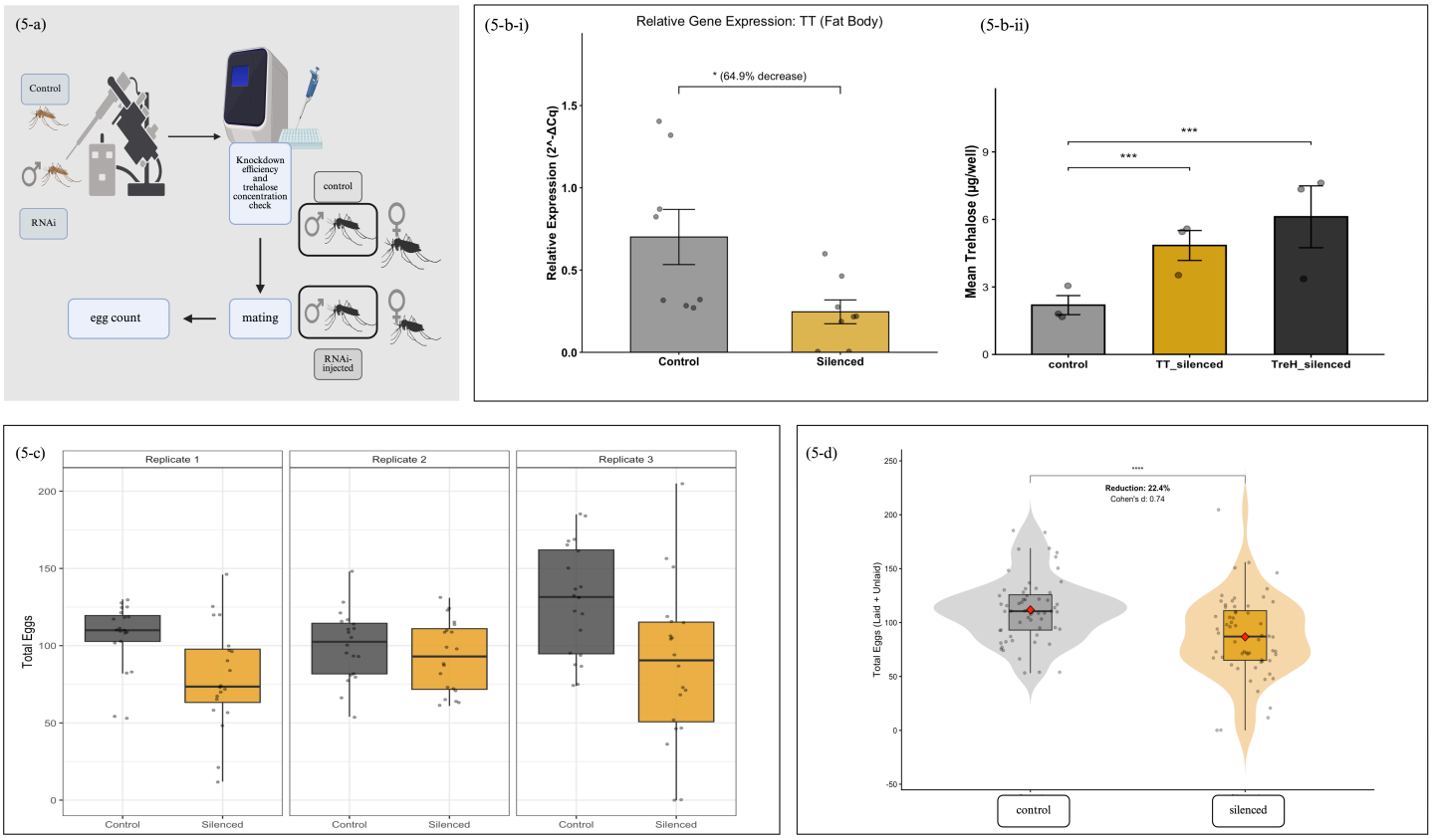


Figure 5

Functional consequences of TreT silencing on trehalose homeostasis and male reproductive output in *Anopheles stephensi*. (a) Experimental workflow illustrating dsRNA-mediated silencing of TreT and TreH in adult males, followed by validation of knockdown efficiency, haemolymph carbohydrate quantification, mating assays, and egg-count analysis. (b-i) TreT transcript levels in fat body tissue following RNAi treatment. TreT expression is significantly reduced in TreT-silenced males compared to controls (Welch's t-test: $t = 2.62$, $df = 7.36$, $p = 0.033$). Individual points represent biological replicates. (b-ii) Haemolymph trehalose concentrations in control, TreT-silenced, and TreH-silenced males. TreT silencing results in a significant increase in circulating trehalose relative to controls ($p = 2.1 \times 10^{-4}$), with a further increase observed following TreH silencing ($p = 6.4 \times 10^{-5}$). (c) Total egg counts from females mated with control

or TreT-silenced males across three independent biological replicates. Boxplots show median and interquartile range with individual data points overlaid.

(d) Combined analysis of total eggs produced per female after mating with control or TreT-silenced males. Females mated with TreT-silenced males produced significantly fewer eggs than controls (paired Student's t-test: t = −3.19, df = 31, p = 0.0033; Wilcoxon signed-rank test: p = 0.0024), corresponding to an approximate 20–22% reduction in egg output (Cohen's d = 0.69).

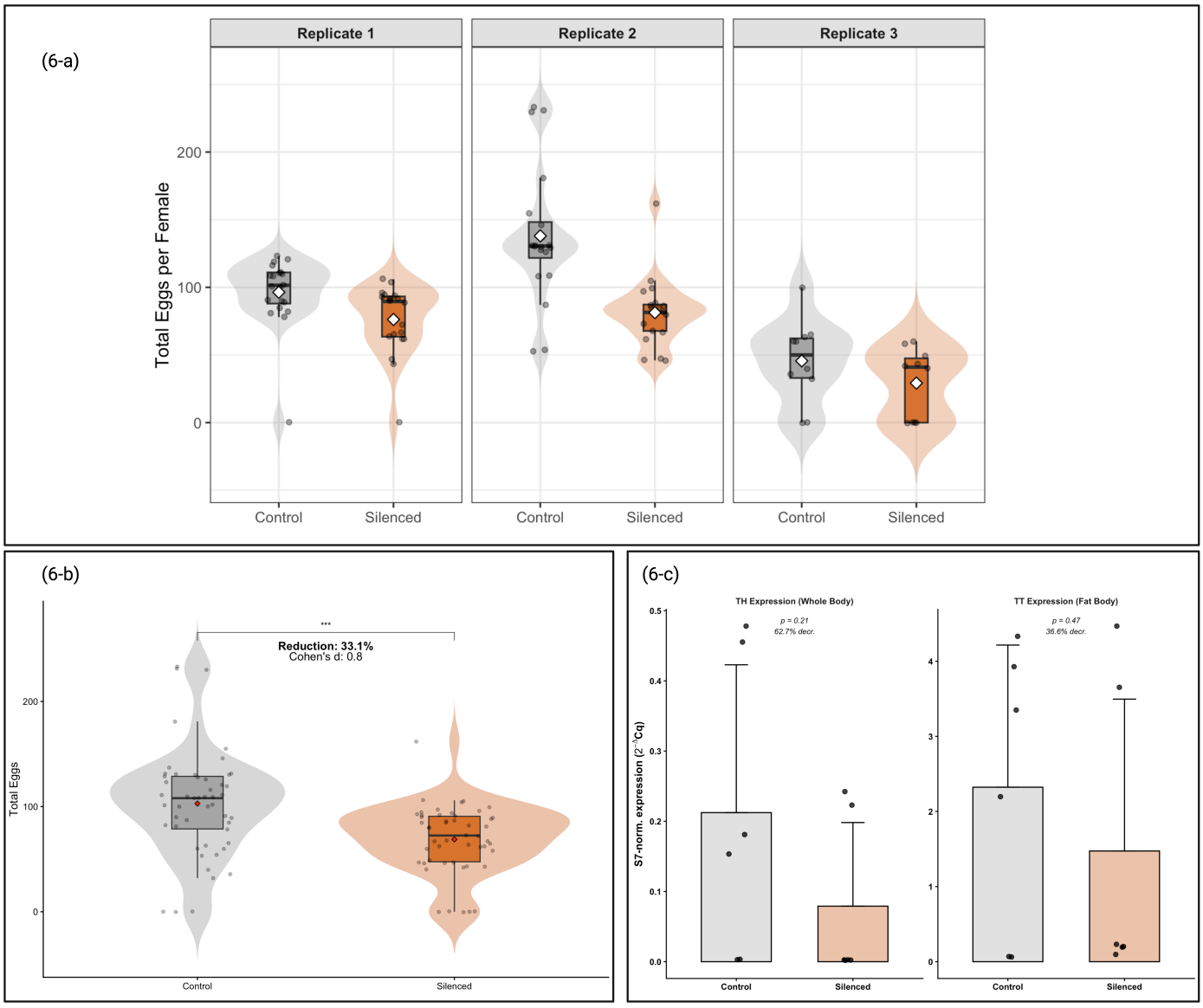


Figure 6

Combined disruption of trehalose transport and hydrolysis exacerbates reductions in male reproductive output.

(a) Total egg output per female following mating with control or double-silenced males (TreT + TreH), shown separately for three independent biological replicates. Violin plots display the distribution of egg counts with embedded boxplots (median and interquartile range) and individual data points. **(b)** Pooled

analysis of total egg output across replicates. Females mated with double-silenced males produced significantly fewer eggs than controls, corresponding to a 33.1% reduction in egg output (**$p < 0.001$), with a large effect size (Cohen's $d = 0.8$). **(c)** Validation of knockdown efficiency following double silencing. TreH expression (whole body) shows a 62.7% reduction ($p = 0.21$), and TreT expression (fat body) shows a 36.6% reduction ($p = 0.47$), indicating partial but variable suppression of both targets. Expression values are normalized to S7, and individual points represent biologicalreplicates.

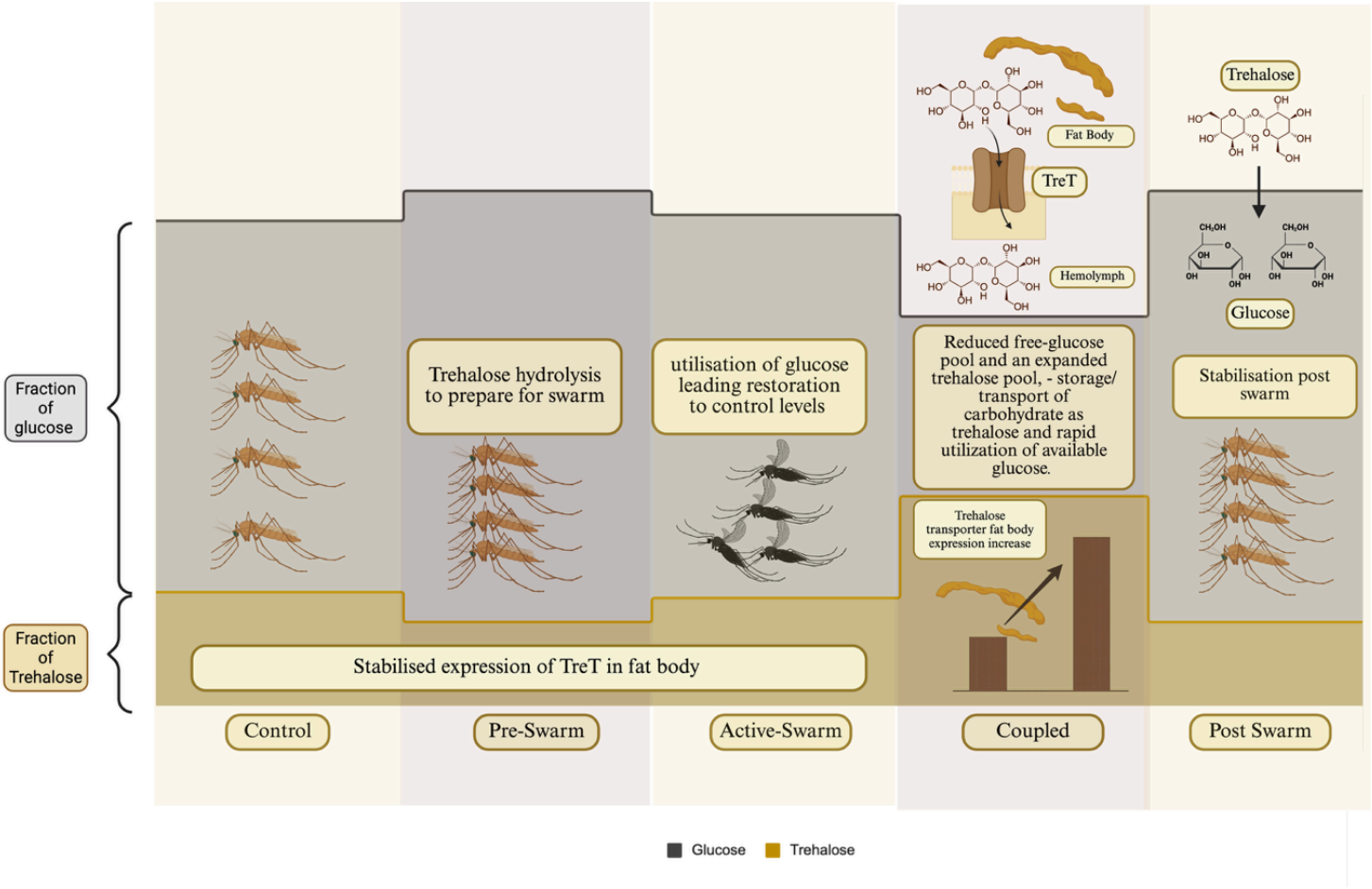


Figure 7

Stage-dependent regulation of trehalose flux in male *Anopheles stephensi*. Schematic model of carbohydrate dynamics across the swarm–mating sequence. The stacked area graph illustrates the relative fraction of haemolymph glucose and trehalose at each behavioural stage. Trehalose hydrolysis predominates during active swarming to support flight, whereas coupling is associated with increased fat body TreT expression and expansion of the trehalose fraction. Post-swarm levels stabilise. TreT disruption uncouples circulating trehalose from tissue utilisation, impairing reproductive performance despite elevated haemolymph trehalose.

Supplementary Files

This is a list of supplementary files associated with this preprint. Click to download.

- SupplementarymaterialTreT13032026.pdf